

RESEARCH ARTICLE

Multienzyme activity profiling for evaluation of cell-to-cell variability of metabolic state

Govind S. Gill^{1,2} | Michael C. Schultz¹ 

¹Department of Biochemistry,
University of Alberta, Edmonton,
Alberta, Canada

²Department of Pediatrics & Group
on the Molecular and Cell Biology
of Lipids, University of Alberta,
Edmonton, Alberta, Canada

Correspondence

Michael C. Schultz, Department of
Biochemistry, University of Alberta,
Edmonton, Alberta, Canada.
Email: michael.schultz@ualberta.ca

Abstract

In solid organs, cells of the same “type” can vary in their molecular phenotype. The basis of this state variation is being revealed by characterizing cell features including the expression pattern of mRNAs and the internal distribution of proteins. Here, the variability of metabolic state between cells is probed by enzyme activity profiling. We study individual cells of types that can be identified during the post-mitotic phase of oogenesis in *Xenopus laevis*. Whole-cell homogenates of isolated oocytes are used for kinetic analysis of enzymes, with a focus on the initial reaction rate. For each oocyte type studied, the activity signatures of glyceraldehyde 3-phosphate dehydrogenase (GAPDH) and malate dehydrogenase 1 (MDH1) vary more between the homogenates of single oocytes than between repeat samplings of control homogenates. Unexpectedly, the activity signatures of GAPDH and MDH1 strongly co-vary between oocytes of each type and change in strength of correlation during oogenesis. Therefore, variability of the kinetic behavior of these housekeeping enzymes between “identical” cells is physiologically programmed. Based on these findings, we propose that single-cell profiling of enzyme kinetics will improve understanding of how metabolic state heterogeneity is related to heterogeneity revealed by omics methods including proteomics, epigenomics, and metabolomics.

KEYWORDS

cell-to-cell variability, development, enzyme, glyceraldehyde 3-phosphate dehydrogenase, kinetic analysis, malate dehydrogenase 1, metabolism, oogenesis, single-cell analysis

1 | INTRODUCTION

Much of what is being done to understand organ functions focuses on characterization of the “types” of cells they include. A recent development has been to try to decipher how single cells of the same type can diverge in their “state.”^{1–3} We already know that variability of state is physiologically meaningful. For example, the metabolic state of

hepatocytes varies according to their location along the axis of liver lobules that extends between the central and portal veins, and this diversity of state is a hallmark of normal liver function.⁴ This paper focuses on the potential utility of single-cell analysis of enzyme kinetics for probing the diversity of metabolic state of post-mitotic cells of the same type.

The nature of state differences between individual cells is now being explored using a plethora of high throughput

This is an open access article under the terms of the [Creative Commons Attribution-NonCommercial-NoDerivs](https://creativecommons.org/licenses/by-nc-nd/4.0/) License, which permits use and distribution in any medium, provided the original work is properly cited, the use is non-commercial and no modifications or adaptations are made.

© 2022 The Authors. *FASEB BioAdvances* published by Wiley Periodicals LLC on behalf of The Federation of American Societies for Experimental Biology.

analytical methods. With respect to metabolism, characterization of cell state can involve integration of data obtained by single-cell measurements of metabolite, mRNA, and protein abundance with existing knowledge of metabolism, including the kinetic properties of enzymes revealed by studying purified proteins.^{5,6} Biochemical estimation of enzyme kinetics for individual cells could conceivably complement such approaches,⁷ but has not been widely used since an early proof of concept study using lysates of isolated hepatocytes.⁸ Therefore, it remains unclear if whole-cell biochemical profiling of enzyme kinetics will yield much more than a catalog of enzymes that can vary in state between cells of a specific type. Most importantly, it is not known if this approach can be used to distinguish variability as biochemical noise buffered by crosstalk in the control system of metabolism from variability that is programmed to increase cell fitness. Here, we address this knowledge gap using a model system approach.

In our approach, the cell type used for enzyme analysis is the *Xenopus laevis* oocyte.⁹ At full size, it has the same volume as approximately 10^6 typical somatic cells.¹⁰ Pilot work revealed that size is an important advantage of this model cell type. Specifically, we found that the homogenate of one isolated full-sized oocyte is sufficient for kinetic analysis of multiple enzymes. A further benefit of using frog oocytes to study single-cell metabolism relates to how oogenesis is programmed in *Xenopus*. Newborn oocytes replicate their DNA and arrest in a G2-like division state. Their subsequent growth and developmental progress are reflected in three overt phenotypes: volume, yolk granule content, and pattern of pigmentation. Based on these phenotypes, oogenesis has been divided into six successive stages (I-VI).¹¹ The overt changes that mark progression through these stages are accompanied by changes of internal molecular phenotype related to metabolic wiring. Progression of cells from stage II to stage III of oogenesis is characterized by a switch in how ATP is generated for glycogen synthesis. Specifically, the fuel source is glucose in stage II and stored yolk proteins thereafter.¹² A hallmark of the stage IV to V transition is acquisition of competence to undergo hormonally stimulated “maturation”. In stage VI oocytes treated with progesterone, this process includes metabolic reprogramming.^{13,14}

We reasoned that cell-to-cell variability of metabolic state could arise during oogenesis because this process involves rewiring of metabolism between developmental stages. To explore this possibility, we probed the metabolic state of individual isolated oocytes at the same stage of oogenesis. Metabolic state was assessed by assaying enzyme activity in whole-cell homogenates. These assays yielded estimates of three Michaelis-Menten parameters: initial reaction rate v_0 , K_m , and V_{max} . They are referred to as $^{cell}v_0$, $^{cell}K_m$, and $^{cell}V_{max}$. The values obtained for these parameters are taken

as signatures of enzyme activity. They are not used to develop mechanistic models of catalysis because enzyme isotypes with different kinetic properties may make up the whole-cell population of an enzyme. Nor are they taken to reveal in vivo flux through GAPDH and MDH1. Rather, their values are compared to address a biological hypothesis related to the proposition that multienzyme activity profiling will advance understanding of cell heterogeneity. The null statement of the biological hypothesis is straightforward: in oocytes of the same type, the potential of a house-keeping enzyme to contribute to metabolism as a catalyst does not vary between individual cells.

Single-cell activity signatures have been obtained for the highly conserved enzymes glyceraldehyde 3-phosphate dehydrogenase and malate dehydrogenase 1 (GAPDH and MDH1). GAPDH is a glycolytic enzyme, and MDH1 is a component of the malate aspartate shuttle.^{15,16} Both are present at high concentrations in the cytosol and nucleus of stage VI oocytes (Figure 1A).^{17,18} There were five important reasons for focusing this test case study on GAPDH and MDH1. 1. Robust activity of these enzymes is detectable upon dilution of whole oocyte lysates into a reaction cocktail based on a physiological homogenization and reaction (HR) buffer. 2. The initial rates of GAPDH and MDH1 can be measured non-invasively by spectrophotometric quantitation of their shared reaction component, NADH (Figure 1A, $\gamma_{max} = 340$ nm). 3. The potential for variability of GAPDH and MDH1 activity state is high because their catalytic properties are controlled by multiple mechanisms. These include acetylation, methylation, and redox state in the case of MDH1.^{19–21} Phosphorylation, acetylation, succination, methylation, malonylation, palmitoylation, RNA binding, and redox state affect GAPDH activity.^{22–29} 4. Covariation of GAPDH and MDH1 activity, which could reflect physiological coupling in the context of metabolism, is highly plausible: both are NAD^+ /NADH-dependent and several existing reports are consistent with their coregulation.^{30–33} 5. Finally, GAPDH and MDH1 are expressed in all analyzed tissues of the human body.³⁴ What is learned about the oocyte enzymes might therefore inform work aimed at characterizing metabolic heterogeneity of other cell types. The results reported below for triplicate assays of GAPDH and MDH1 in 144 individual oocytes from four adult animals indeed encourage this expectation.

2 | MATERIALS AND METHODS

2.1 | Oocyte isolation, maintenance, and imaging

All procedures were performed at room temperature. Ovaries were removed from adult females (*Xenopus*

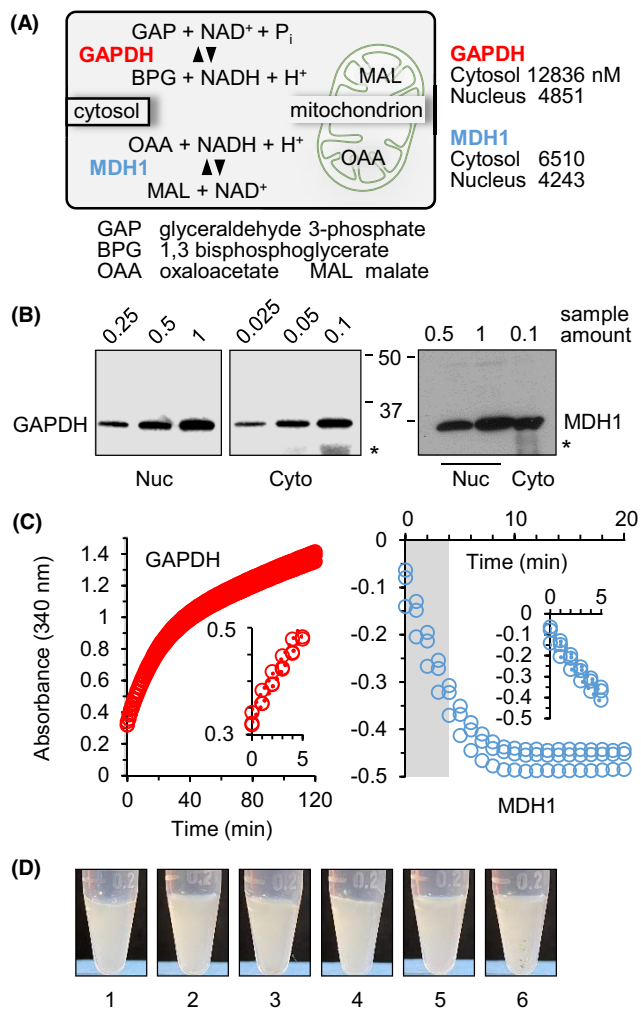


FIGURE 1 Experimental approach for analysis of enzyme activity in single oocytes. (A) Reactions catalyzed by cytosolic GAPDH and MDH1. Enzyme concentrations in the oocyte nucleus and cytoplasm are from Kirli et al. (B) GAPDH (35,698 kDa) and MDH1 (36,425 kDa) are abundant in the oocyte. Isolated stage VI oocytes were dissected to remove the nucleus and therefore obtain samples of whole nuclei (Nuc) and whole cytoplasms (Cyto) for Western blotting analysis. As expected, both enzymes are present in the nucleus and cytoplasm.^{17,18} Sample amount 1 = content of 1 nucleus or cytoplasm. *cross-reacting bands likely are processing products of vitellogenin, which oocytes take up by endocytosis. The GAPDH lanes are from a single blot. (C) Representative progress curves for GAPDH (left) and MDH1 (right) activity in homogenate of a single-stage VI oocyte. The pullouts show NADH synthesis (GAPDH) and consumption (MDH1) during the first 5 min of the reactions; these data were obtained in triplicate and the slopes of the linear trendlines averaged to obtain the initial reaction rate for the pool of an enzyme in a whole cell. This estimate is referred to as $^{cell}v_0$. The A_{340} readings for MDH1 progress curves are brought into the negative range by subtraction of the blanks. (D) Homogenates of six stage VI oocytes. Samples of these turbid homogenates were diluted for enzyme assays.

One, MI, U.S.A.) according to a protocol approved by the Health Sciences Animal Care and Use Committee of the University of Alberta (AUP 0000942). In this protocol,

animals are anesthetized using tricaine methanesulfonate and then euthanized by decapitation. Oocytes were released from their follicles by collagenase treatment (2 h with 3 mg/ml collagenase and 1 mg/ml bovine serum albumin [BSA] in OR-2 medium; 5 mM Hepes-NaOH pH 7.8, 82.5 mM NaCl, 2.5 mM KCl, 1 mM MgCl₂, 1 mM CaCl₂, 1 mM Na₂HPO₄).³⁵ Somatic cells still associated with oocytes were then removed by gentle rocking on a sandpaper surface under OR-2 medium (Liu and Liu, 2006).³⁶ DAPI staining (1 mg/ml) of randomly selected oocytes confirmed detachment of somatic cells. Oocytes were maintained in OR-2 with penicillin and streptomycin (100 µg/ml each) until use within 3 day after isolation. They were imaged using a MZ6 dissecting microscope, IC90 E camera, and Application Suite v.4.12.0 (Leica). Oocyte diameter was estimated from these images.

2.2 | Preparation of single-cell homogenates

Individual oocytes were washed in fresh OR-2 and then placed into “Homogenization and Reaction” (HR) buffer. HR buffer is “Isolation Medium with Mg²⁺” (IM; 83.0 mM KCl, 17.0 mM NaCl, 6.5 mM Na₂HPO₄, 3.5 mM KH₂PO₄, 1.0 mM MgCl₂, pH 7.4)³⁷ supplemented with 20% glycerol and 1 mM dithiothreitol (DTT). Stage IV and VI cells in 13.4 and 50 µl HR, respectively, were dispersed by 5 gentle up-and-down pipettings into a 200 µl pipette tip and then 5 s of vortexing at 3200 rpm. Stage II cells were processed differently because of their small size. They were manually broken open in 5 µl HR using a P10 pipette tip (this was done under a dissecting microscope). This was followed by 5 gentle up-and-down pipettings into a P10 tip, addition of a further 5 µl of HR, and 5 s of vortexing at 3200 rpm. Homogenates of individual oocytes were stored at −80°C until use.

2.3 | Enzyme activity measurement and estimation of kinetic parameters

All assays were performed in Corning® 384 Well Deep Well Plates (Sigma CLS3347) using a BioTek Synergy 4 with Hybrid Technology™ plate reader. After thawing, oocyte homogenates were diluted on ice with HR buffer (ice-cold) and manually added to plate wells. The fraction of a single cell (by volume) that was assayed is as follows. GAPDH: Stage II—0.0512; stage IV—0.0032; stage VI—0.0032. MDH1: Stage II—0.0512; stage IV—0.0064; stage VI—0.0064. These cell amounts were dispensed in 10 and 20 µl for GAPDH and MDH1, respectively. The reader was configured to inject a cocktail containing the

additional required reagents (substrates) and bring the final reaction volume to 40 μ l. All reactions were performed in triplicate at room temperature, and absorbance at 340 nm was recorded every minute. For GAPDH, all assays were in IM containing 5% glycerol, 10 mM arsenate, and 1 mM DTT. Arsenate was included to inhibit GAP consumption.³⁸ The substrate concentrations used were 6 mM NAD⁺/2 mM GAP (animals 1, 4) and 1 mM NAD⁺/1 mM GAP (animals 2,3). The blanks for the GAPDH activity assay contained oocyte homogenate but no substrates. All MDH1 assays were performed in IM with 10% glycerol and 1 mM DTT. The substrate concentrations used were 0.25 mM NADH/0.075 mM OAA (animals 1, 4) and 0.2 mM NADH/0.25 mM OAA (animals 2,3). The MDH1 blanks contained substrates but no cell homogenate (animals 2, 3) or cell homogenate and NADH, but no OAA (animals 1, 4). To assess technical reproducibility, enzyme assays were performed in 18 wells (in triplicate) loaded with the same whole-cell extract. Initial reaction rates were obtained from the data for the first five minutes of a reaction. The plots of MDH1 $^{cell}v_0$ at different OAA concentrations were analyzed using a nonlinear regression method for estimation

of Michaelis-Menten kinetic parameters (GraphPad Prism 9). A thorough discussion of the merits of this fitting method for estimating K_m and V_{max} is available in Kemmer and Keller (2010).³⁹ Varying the conditions of assay did not affect any of the conclusions drawn in this study. Importantly, technical reproducibility for stage VI homogenates varied little between the sets of conditions used (GAPDH for animals 1, 4 and 2, 3: relative standard deviation of $v_0 = 2.08$ and 2.70%, respectively; MDH1 for animals 1, 4 and 2, 3: relative standard deviation of $v_0 = 2.77$ and 2.74%, respectively). Interestingly in the experiment in Figure 2A, the average activity of MDH1 for samples of the technical replicate homogenate (0.027 $\Delta A_{340nm}/min$) was higher than the average activity for the 18 individual cell homogenates (0.010 and 0.009 $\Delta A_{340nm}/min$, animals 2 and 3). This difference may be due to the subtly different physical conditions for homogenization of individual cells (single-cell analysis) and pools of 18 cells (technical replicate sample). For single-cell analysis, oocytes were homogenized in a small volume of buffer in 600 μ l tubes. The technical replicate samples were prepared in an 18-fold more buffer in a 1.5 ml tube. Thus, the preparation of the single-cell and

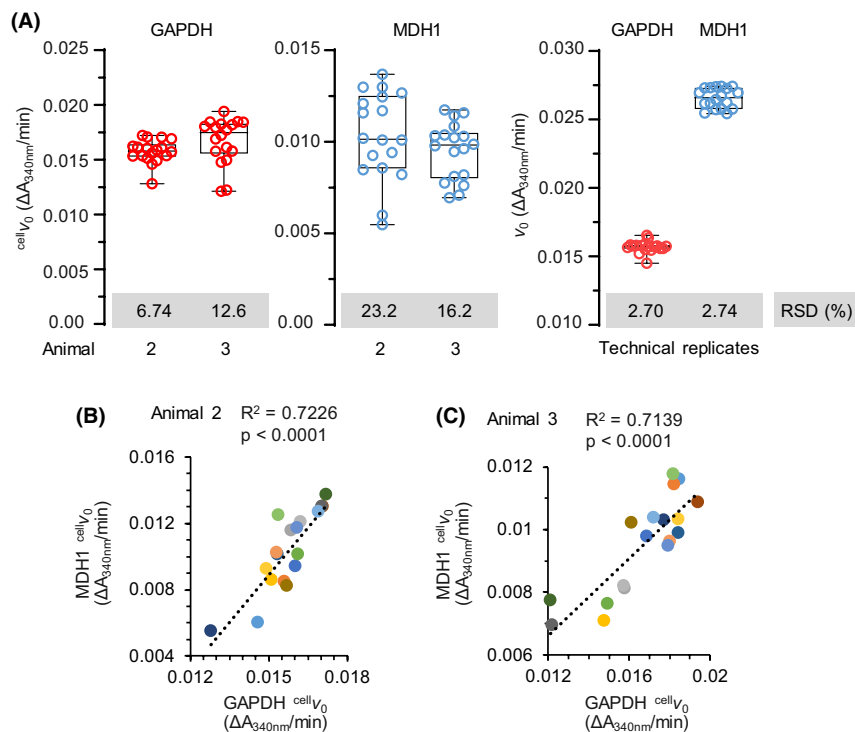


FIGURE 2 Variability of GAPDH and MDH1 $^{cell}v_0$ (whole-cell initial rate) in individual stage VI oocytes. (A) Two sets of 18 oocytes were analyzed, each from a different animal. Each oocyte homogenate was assayed separately for GAPDH and MDH1 activity to obtain $^{cell}v_0$ as the change in absorbance at 340 nm with time ($\Delta A_{340}/min$). The $^{cell}v_0$ data for GAPDH and MDH1 are shown in the left and middle panels, respectively. Technical reproducibility (right panel) was assessed by assaying enzyme activity in 18 aliquots of a control homogenate prepared from multiple oocytes. RSD, relative standard deviation (shaded in gray). (B) Relationship between variability of GAPDH and MDH1 $^{cell}v_0$ in individual stage VI oocytes of animal 2 of this study. (C) Relationship between variability of GAPDH and MDH1 $^{cell}v_0$ in individual stage VI oocytes of animal 3 of this study. In panels B and C, dot colors for individual cells were randomly assigned by Excel.

technical replicate homogenates differed with respect to homogenization tube size, geometry, and homogenate volume relative to tube volume. These differences could have affected the amount of MDH1 activity detectable in the lysates. No such effect is observed for GAPDH, which served as the test enzyme when we developed the homogenization methods. We have not tested alternative methods for preparing the technical replicate sample.

2.4 | Western blotting

Whole oocyte nuclei and cytoplasms were dispersed and diluted in HR buffer. After addition of 5X load buffer (0.25 M Tris-HCl pH 6.8, 10% wt/vol SDS, 50% vol/vol glycerol, 0.5 M DTT, 0.25% wt/vol bromophenol blue), 12.5 μ l samples were denatured for 15 min at 65°C and resolved in SDS-12% polyacrylamide gels. Proteins were blotted to nitrocellulose in 25 mM Tris base, 190 mM glycine, 20% methanol (pH 8.2) using a Bio-Rad submarine transfer module (GAPDH, overnight in cold cabinet; MDH1, 1 hr with ice cooling). TBS with 0.1% Tween 20 and 4% BSA (TBST) was used for blocking (GAPDH, 1 hr at room temperature; MDH1, overnight in cold cabinet). Blots were incubated for 30 min in primary antibody in blocking buffer at room temperature. GAPDH: 1:2000 mouse monoclonal antibody raised against recombinant human GAPDH (sc-47724, Santa Cruz Biotechnology Inc., note that human and *X. laevis* GAPDH are 81% identical and 90% similar).⁴⁰ MDH1, 1:500 mouse monoclonal antibody raised against a segment of human MDH1 with 91% identity to *X. laevis* MDH1 (sc-166879, Santa Cruz Biotechnology Inc., details courtesy of the supplier). The secondary antibody was goat anti-mouse IgG (H+L)-HRP conjugate (1706516, Bio-Rad) at 1:2000 (GAPDH) and 1:8000 (MDH1) in TBST. Signals generated by incubation in Amersham™ ECL™ Western Blotting Detection Reagents were captured on film.

2.5 | Oocyte fractionation and proteome analysis

Isolated stage V oocytes (end of stage V in pigmentation and start of stage VI in size) were dissected under mineral oil (Sigma M-5904) according to Paine et al. to obtain near-native nuclei and cytoplasms.⁴¹ Whole cytoplasms were dispersed in HR buffer (1 cytoplasm/25 μ l HR buffer) and centrifuged at 4°C (7,500 \times g, 15 min) for collection of the S7500 supernatant. The proteome of six individual cytoplasmic S7500s was determined by LC-MS as previously described for whole cells.⁴² Relative abundance values as % of total \sum #PSMs were ranked using the PERCENTRANK.EXC function in Excel 2016.

3 | RESULTS

3.1 | Cell isolation, homogenate preparation, and enzyme assays

Oocytes were isolated from animals by collagenase digestion of ovary fragments and rolling on sandpaper to remove all adherent somatic cells.³⁶ The latter step minimized possible corruption of oocyte enzyme activity data by enzymes in other cells. Oocytes are spherical cells. They were photographed before homogenization so that their volumes could be determined and related to enzyme activity on a cell-by-cell basis. Consistent with recent characterizations of the *Xenopus* oocyte proteome,^{17,18} full-length GAPDH and MDH1 were readily detected by Western blotting analysis of ensemble homogenates (Figure 1B).

In vitro assays for GAPDH and MDH1 activity were established using representative homogenates of stage II, IV, and VI oocytes. The amount of HR buffer for homogenization of stage IV cells was scaled to obtain the same buffer: cell volume ratio as one stage VI oocyte/50 μ l buffer. Cell dispersion was limited to gentle pipetting and vortexing. GAPDH was assayed in the direction of NADH synthesis (GAP consumption), and MDH1 activity was assayed in the direction of NADH and OAA consumption. Forty μ l assays were performed in 384-well plates with automated substrate injection. For each enzyme, addition of both substrates was required to detect activity. Reactions for comparing $^{cell}v_0$ between oocytes were performed under saturating conditions of substrate and used amounts of homogenate that yielded activity in the midrange of titrations of lysate amount. All progress curves were generated by averaging the data from three reaction replicates. $^{cell}v_0$ data obtained in substrate titrations were used to calculate $^{cell}K_m$ and $^{cell}V_{max}$ using nonlinear regression for data fitting³⁹ as implemented in GraphPad Prism. Representative kinetic data for GAPDH and MDH1 in the homogenate of a single-stage VI oocyte are shown in Figure 1C. The full progress curves are for repeat assays using the same amount of homogenate. The pullouts are NADH abundance change during the linear phase of each reaction (Figure S1 shows such plots for GAPDH and MDH1 in 18 oocyte homogenates). These results met our expectation that GAPDH and MDH1 activity would be readily detected in assays of diluted whole oocyte homogenate. This expectation was encouraged by three facts. First, GAPDH and MDH1 are highly expressed in the oocyte (Figure 1A). Second, metabolic tracer studies of isolated oocytes have revealed high flux through GAPDH, and high respiratory activity which would require operation of the MDH1-dependent malate aspartate shuttle (Dworkin and Dworkin-Rastl, 1989).¹² Finally, robust activity of NAD⁺/NADH-dependent enzymes has been obtained

using whole-cell homogenates of mammalian cell populations (Board et al., 1990).⁴³

3.2 | Assessment of variability

Sets of 18 cells at the indicated stages of oogenesis were used to assess variation of $^{cell}v_0$. This sample size was chosen based on the results of a study in which cell-to-cell heterogeneity of the response to progesterone was revealed by studying groups of 14–19 oocytes.⁴⁴ The variation of $^{cell}v_0$ between cell homogenates is reported as relative standard deviation, ^{cell}RSD . To evaluate the possible biological meaning of any particular ^{cell}RSD value, it is necessary to know the technical reproducibility of the assay (^{tr}RSD). ^{tr}RSD could be obtained from v_0 measurements of samples from a stock solution of purified enzyme. Such an estimate, however, is unlikely to be meaningful with regard to enzyme activity in homogenates. That is because oocyte lysates are very inhomogeneous compared to solutions of purified enzyme. They contain the entire contents of the cell and are turbid to the naked eye (Figure 1D shows six stage VI homogenates). Therefore, in our experiments, ^{tr}RSD was obtained from 18 measurements of v_0 for a single control homogenate. Separate ^{tr}RSD estimates were made for stage II, IV, and VI control homogenates.

3.3 | Cell-to-cell variability of enzyme activity signatures in isolated stage VI oocytes

Estimates of $^{cell}v_0$ for GAPDH and MDH1 in full-grown oocytes of two animals are shown in the box and whisker plots in Figure 2A (left and middle panels). The right panel shows v_0 data for the technical replicates. We first consider GAPDH (Figure 2A, red plots). The mean v_0 for the 18 technical replicate determinations of GAPDH activity is similar to the mean v_0 for each set of 18 homogenates (0.016 compared to 0.017 and 0.019 ΔA_{340} nm/min). Despite this similarity, the variability of v_0 is much higher for each set of individual oocytes than for repeat sampling of the single control homogenate. Specifically, the $^{cell}RSDs$ are 6.74 and 12.6% while the ^{tr}RSD is 2.70% (Figure 2A, gray boxes). For animals 2 and 3, respectively, the variability of GAPDH $^{cell}v_0$ is 2.5- and 4.7-fold higher than technical variability. It follows that oocytes at the same stage of development and cell cycle position are not uniform with regard to the activity signature of their whole population of GAPDH molecules.

The homogenates that were used to assess GAPDH activity were also assayed for MDH1 activity (Figure 2A, blue plots). The control homogenate has a higher mean v_0 for MDH1 than GAPDH (Figure 2A, right panel). Assay

reproducibility, however, is similar for these enzymes ($^{tr}RSDs$ of 2.70 and 2.74%, respectively). The variability of MDH1 $^{cell}v_0$ between oocyte homogenates is 8.5- and 5.9-fold higher than technical variability for MDH1 (Figure 2A, compare RSD values in middle and right-most panels). Therefore, stage VI oocytes vary in the activity signatures of both MDH1 and GAPDH.

From the data for each enzyme on its own, we cannot say if the variability of $^{cell}v_0$ is likely: (1) to underlie physiologically meaningful divergence of metabolic programming between cells, or (2) reflect in vivo biochemical noise. We therefore generated scatterplots of the data for animals 2 and 3 to visualize the extent of covariation of GAPDH and MDH1 $^{cell}v_0$ (Figures 2B,C; each data point is a cell). The cell-by-cell correlation of GAPDH and MDH1 activity is very high for both animals ($R^2 = 0.7226, 0.7139$). In other words, when GAPDH activity is high in a cell, so is MDH1 activity. This correlation would not be observed if $^{cell}v_0$ for these enzymes fluctuates randomly. We conclude that a biochemical control mechanism couples GAPDH and MDH1 activity state in isolated stage VI oocytes. It follows that variability of metabolic state revealed by estimating the $^{cell}v_0$ of housekeeping enzymes GAPDH and MDH1 is a physiologically meaningful axis of phenotypic heterogeneity of the full-grown oocyte.

One mechanism that could at least partly underlie the covariance of $^{cell}v_0$ for GAPDH and MDH1 in oocytes would be co-regulation of enzyme expression. This possibility is supported by the results of an experiment in which the proteomes of a low-speed supernatant from individual cytoplasms were characterized by liquid chromatography coupled to tandem mass spectrometry (LC-MS; data in Table S1). Late-stage V oocytes were used. They were dissected under oil to obtain whole nuclei and cytoplasms.⁴¹ Centrifugation of cytoplasmic homogenates at 7500 x g yielded the low-speed supernatants (S7500s) for analysis of cytoplasmic proteins. Analysis of cytoplasmic S7500s was advantageous because yolk granule depletion reduces the signal from vitellogenins which comprise approximately 90% of total oocyte protein.^{45,46} The relative abundance of a protein was estimated by spectral counting; for each sample, it is expressed as % of total Σ peptide spectral matches (PSMs). The within-sample ranking of these abundance estimates was also determined (% rank).

In this sample set, cross-contamination of cytoplasm with nuclear material was minimal (compartment markers NASP and EEF2.1, Figure 3A). All cytoplasmic S7500s contained GAPDH and MDH1, and the abundance of each enzyme differed substantially between many individual cytoplasmic S7500s (Figure 3B). Considering this variability, it is striking that MDH1 expression is lower than GAPDH in every cytoplasm, and that GAPDH and MDH1 strongly co-vary in abundance. For example, GAPDH abundance is at its highest and lowest in cytoplasms 1 and

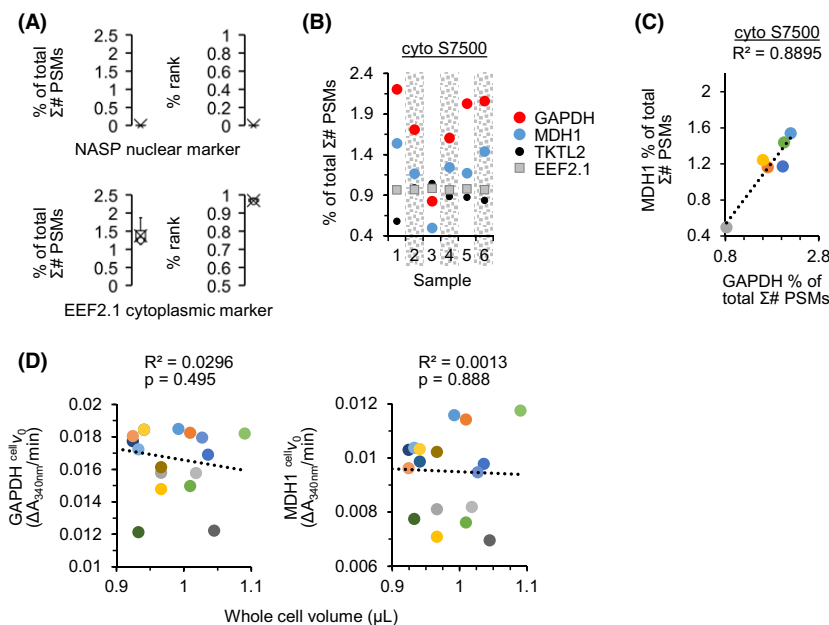


FIGURE 3 Enzyme expression level in individual cytoplasms and relationship of $^{cell}v_0$ to cell volume. (A) Compartment markers NASP (Nuclear Autoantigenic Sperm Protein, nucleus) and EEF2.1 (Eukaryotic Translation Elongation Factor 2.1, cytoplasm) have the expected expression level in the cytoplasm. Six oocytes (late stage V) were dissected to obtain near-native nuclei and cytoplasms. The low-speed supernatants of individual cytoplasms (cyto S7500) were then analyzed by LC-MS to obtain their proteomes. Protein abundance was estimated by spectral counting (% of total Σ # PSMs) and ranked according to these estimates (%rank). (B) Relative expression of GAPDH and MDH1 in isolated cytoplasms (GAPDH, red dots; MDH1 blue dots). Fluctuation of GAPDH abundance is matched by fluctuation of MDH1 abundance. TKTL2, a pentose phosphate pathway enzyme, does not co-vary with either GAPDH or MDH1. For example, TKTL2 expression is lower than GAPDH and MDH1 in cytoplasm 1, but higher than both in cytoplasm 3. The expression level of translation factor EEF2.1 is remarkably similar in the cytoplasms analyzed. (C) Relationship between the abundance of GAPDH and MDH1 (% of total Σ # PSMs) in isolated cytoplasms. (D) Relationship between $^{cell}v_0$ and cell volume for 18 stage VI oocytes (animal 3). Each dot is an individual cell. Equations for the lines of best fit in 3C and D are presented in Table S2A,B.

3, respectively. These cytoplasms also rank as the highest and lowest for MDH1 expression. The positive correlation of GAPDH and MDH1 abundance is readily apparent in a scatterplot of the data (Figure 3C, $R^2 = 0.8895$). Since $^{cell}v_0$ for GAPDH and MDH1 also co-vary (Figure 2B, C), it is plausible that co-regulation of enzyme expression level in the cytoplasm (Figure 3C) partly underlies the co-regulation of v_0 for GAPDH and MDH1 in whole-cell homogenates. This possibility is strengthened by the fact that the cytoplasmic pools of GAPDH and MDH1 account for 96 and 94%, respectively, of the total cellular amount of these enzymes (calculations based on published ensemble protein concentration data and compartment volume estimates).¹⁷ Interestingly, a study of 16 individual stage VI oocytes revealed low cell-to-cell variability of GAPDH mRNA expression compared to several other genes that have not been assigned housekeeping functions (e.g., *stat3* and *pdk3*).⁴⁷ Post-transcriptional mechanisms may therefore underlie the heterogeneity of GAPDH protein expression revealed by our analysis.

For GAPDH and MDH1, the strength of correlation of $^{cell}v_0$ ($R^2 = 0.7226$ and 0.7139 ; Figure 2B, C) is lower than for abundance of these enzymes ($R^2 = 0.890$; Figure 3C).

This fact raises the possibility that the activity of either GAPDH or MDH1 is limited (or induced) by a mechanism unrelated to its abundance. Based on the observed correlation of enzyme abundance and activity, we predicted that $^{cell}v_0$ for GAPDH and MDH1 would be positively correlated with cell volume. That is, large cells would contain more GAPDH and MDH1 than small cells and therefore yield homogenates with higher values of $^{cell}v_0$. Plots of cell volume against $^{cell}v_0$ for GAPDH and MDH1 reveal this not to be true at stage VI of oogenesis (Figure 3D).

3.4 | Developmental regulation of metabolic state variation: evidence from the analysis of enzyme activity signatures of isolated stage II, IV, and VI oocytes

Some differentiation processes are characterized by dynamic changes in the variability of mRNA expression.^{48–52} This fact prompted us to explore the possibility that fluctuation of variability of GAPDH and MDH1 $^{cell}v_0$ is a hallmark of oocyte development. Homogenates were prepared

from cells at stages II, IV, and VI of oogenesis.¹¹ Some important distinguishing features of stage II, IV, and VI oocytes are as follows. Stage II oocytes are 300–450 μm in diameter. They are translucent because their content of yolk and pigment granules is very low. Stage IV oocytes are 600–1000 μm in diameter and heavily pigmented. They contain an abundance of yolk granules. Stage VI oocytes have reached the full size of the lineage (1200–1300 μm diameter). Their pattern of pigmentation and yolk granule content are stable over time. Developmental regulation of enzyme activity signature was studied in cells from two animals (Figure 4, animals 1 and 4; note that stage VI cells analyzed in Figures 2 and 3 above were from animals 2 and 3). For each animal, staged oocytes were processed at the same time after isolation.

The workflow for collection of stage-specific $^{\text{cell}}v_0$ data started with standardization experiments using stage-specific control lysates. These titration experiments established the volume of homogenate that yielded a midrange v_0 value for each enzyme at each developmental stage. These volumes differed between stages, and for the same control lysate, the volumes differed between GAPDH and MDH1. Our goal to characterize cell-to-cell variability of whole-cell enzyme activity (rather than enzyme mechanisms) is not affected by these differences. It is worth noting that standardization to lysate protein concentration is not appropriate for comparison of cells at different stages of oogenesis. That is because the total protein content of oocytes increases dramatically after stage II owing mainly to yolk protein (vitellogenin) accumulation in membrane-bound yolk granules. These organelles are virtually absent at stage II but occupy half the volume of the oocyte at stage VI.⁴⁶ It follows that assaying the same protein amount of stage II and stage VI homogenate would be associated with severe under-sampling of cytosolic proteins at stage VI.

The developmental analysis of variability of GAPDH and MDH1 $^{\text{cell}}v_0$ in different oocyte types included stage-matched control experiments. These technical replicate experiments assessed initial rate variation associated with repeat sampling of ensemble homogenates of each oocyte type. The latter were prepared from pools of staged oocytes by scaled up versions of the methods used to process single cells. Eighteen aliquots were taken from each technical replicate homogenate. These aliquots were then subsampled for assay of GAPDH and MDH1 activity. For each enzyme, the volume of control lysate assayed was the same as the volume used to assay single-cell homogenates.

The $^{\text{cell}}v_0$ data for stage II, IV, and VI oocytes of animals 1 and 4 are shown in Figure 4A, along with the data for the technical replicate controls. Figure 4B is a bar graph of the $^{\text{cell}}\text{RSD}$ and $^{\text{tr}}\text{RSD}$ values in Figure 4A ($^{\text{cell}}\text{RSD}$ as solid bars compared to $^{\text{tr}}\text{RSD}$ as hatched bars; GAPDH in red

and MDH1 in blue). At each development stage examined, the heterogeneity of GAPDH and MDH1 activity obtained by measuring $^{\text{cell}}v_0$ of individual oocytes is greater than the heterogeneity observed for multiple samples of a control homogenate (Figure 4B). High variability of $^{\text{cell}}v_0$ for GAPDH and MDH1 is therefore a general feature of cells in the oocyte lineage. Remarkably, the magnitude of variability is not fixed during development. The strong trend is for $^{\text{cell}}v_0$ heterogeneity to decline as oocytes progress from stage II to stage VI of oogenesis. This is true for both MDH1 and GAPDH. In the case of MDH1, the decline is steady (Figure 4B, middle panel, blue plots). The decline of $^{\text{cell}}\text{RSD}$ for GAPDH is characterized by a sharp drop between stage II and IV (Figure 4B, red plots in left panel). For animal 1, MDH1 $^{\text{cell}}\text{RSD}$ at stages II and IV is 5.57- and 2.34-fold higher than at stage VI of oogenesis. For animal 4, $^{\text{cell}}\text{RSD}$ at stages II and IV is 6.87- and 2.25-fold higher than at stage VI. A provocative conclusion supported by these data is that a programmed reduction of cell-to-cell heterogeneity of metabolic state is a hallmark of the development of G2-arrested oocytes.

3.5 | The strength of covariation of GAPDH and MDH1 activity signatures depends on oocyte developmental stage

Covariation of GAPDH and MDH1 $^{\text{cell}}v_0$ was visualized for the stage II, IV, and VI oocytes of animals 1 and 4 and the corresponding technical replicate homogenates (Figure 5). No covariation of GAPDH and MDH1 v_0 was associated with subsampling of any control homogenate (Figure 5, plots at right; the highest R^2 was 0.0983). On the contrary, covariation of GAPDH and MDH1 $^{\text{cell}}v_0$ was a prominent within-group feature of oocytes at the three developmental stages examined (Figure 5, left-most and middle columns). That is, the strength of the positive linear correlation between GAPDH and MDH1 $^{\text{cell}}v_0$ was as high as $R^2 = 0.9312$ (stage II, animal 1) and not lower than $R^2 = 0.3927$ (stage IV, animal 4). Surprisingly, the strength of covariation of $^{\text{cell}}v_0$ depended on developmental stage. It was highest in stage II oocytes of both animals ($R^2 = 0.9312$ and 0.7662; Figure 5, top row of plots). For animal 1, the strength of covariation of $^{\text{cell}}v_0$ declined progressively to a minimum at stage VI, while the R^2 values for stage IV and VI oocytes of animal 4 were similar to one another (0.3927, 0.4044) and lower than at stage II. The trend for strength of $^{\text{cell}}v_0$ correlation for GAPDH and MDH1 to decrease with stage of development (Figure 5) is accompanied by a strong trend of decreasing heterogeneity of GAPDH and MDH1 $^{\text{cell}}v_0$ (Figure 4). Thus, stage II oocytes which have the highest variability of GAPDH and MDH1 $^{\text{cell}}v_0$ (Figure 4B, $^{\text{cell}}\text{RSD} = 27.7$ and 37.6%) also have the most robust

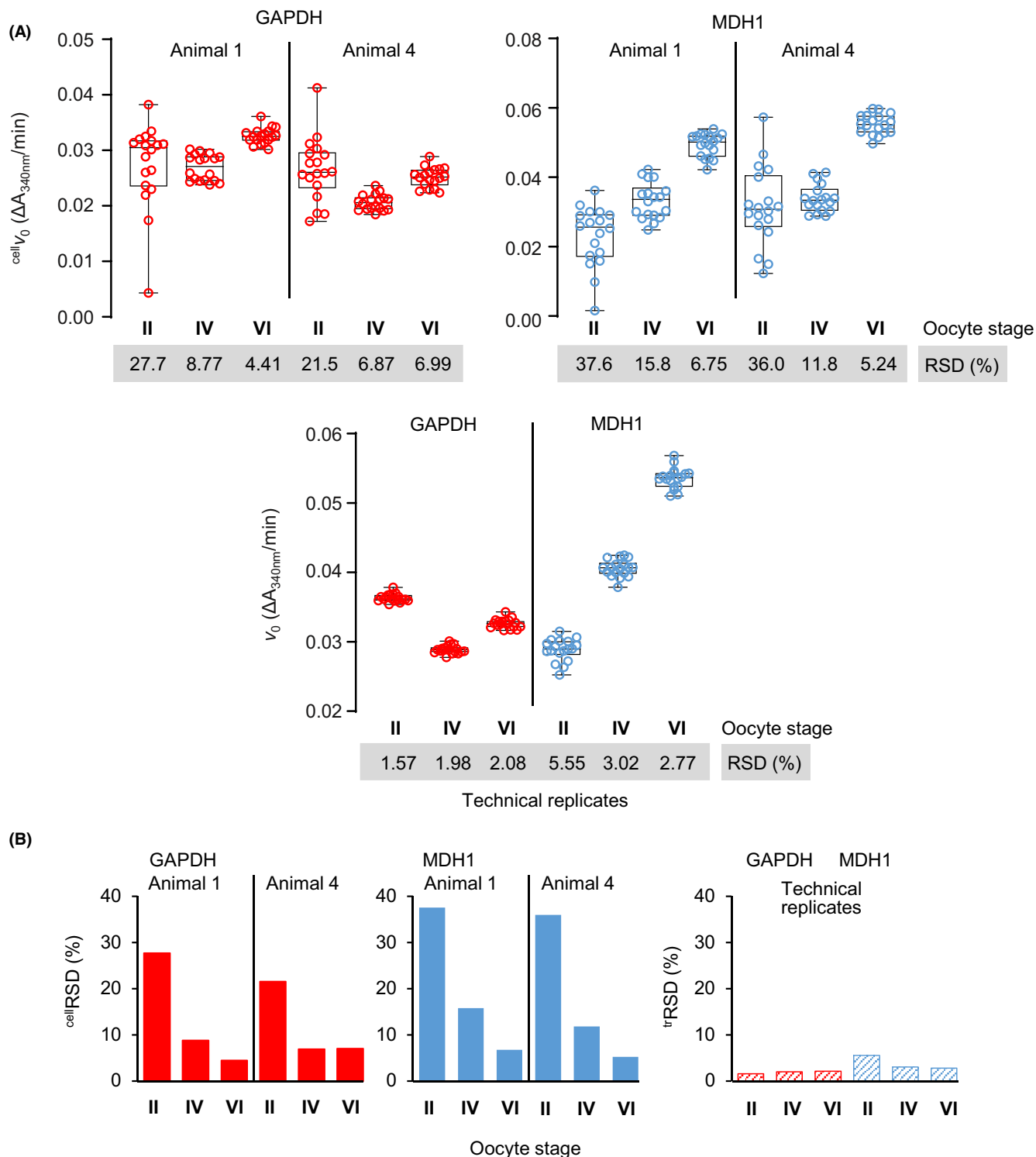


FIGURE 4 Variability of GAPDH and MDH1 $^{cell}v_0$ in individual oocytes of three types. (A) $^{cell}v_0$ was determined for GAPDH (red) and MDH1 (blue) in individual stage II, IV, and VI oocytes from two animals (top two panels; each box and whisker plot shows the data for 18 cells). v_0 for GAPDH and MDH1 was also determined for control ensemble homogenates of the same oocyte types (technical replicates in bottom panel). Variability as relative standard deviation (RSD shaded in gray) is higher for each set of 18 individual oocytes (top panels) than for variability of activity associated with repeat sampling of the corresponding (stage-matched) technical replicate homogenates. For each type of oocyte, the variability of enzyme activity between individual cells was higher than the variability between replicate samples from the corresponding control homogenate. For example, the RSD for GAPDH in the 18 stage II cells of animal 1 was 27.7% (top panel, left-most plot); the RSD for the corresponding technical replicate control was 1.57% (bottom panel, left-most plot). (B) Plots of the relative standard deviation (RSD) associated with assay of GAPDH and MDH1 activity in individual cells (^{cell}RSD , left two panels) and in repeat samples of technical replicate homogenates (^{tr}RSD , right panel). This is a representation of the RSD data in A.

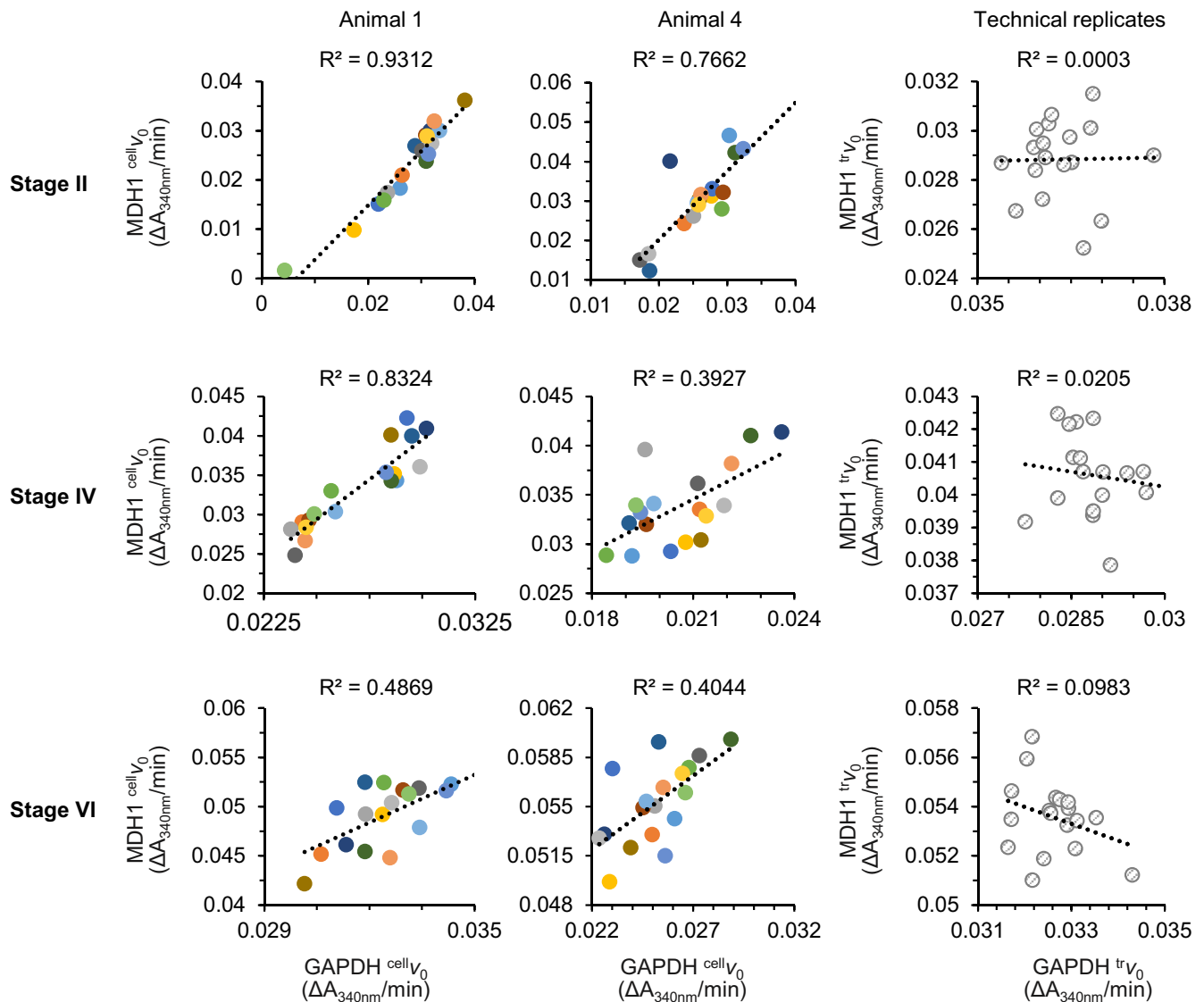


FIGURE 5 Covariation of GAPDH and MDH1 $^{cell}v_0$ for oocytes at three stages of development. The data for individual cells from two animals are shown in the left and middle columns. For the technical replicate controls (plots at right), eighteen aliquots of an ensemble homogenate of the indicated oocyte type were subsampled for separate assays of MDH1 and GAPDH activity. The highest variability of $^{cell}v_0$ was for GAPDH in stage II cells ($R^2 = 0.9312$). For the corresponding control homogenate $R^2 = 0.0003$. Equations for the lines of best fit are provided in Table S2C.

covariation of GAPDH and MDH1 $^{cell}v_0$ (Figure 5; stage II $R^2 = 0.9312$ and 0.8753 compared to stage IV $R^2 = 0.8324$ and 0.3927). This pattern of association between variability among observations and strength of correlation is expected when the conditions appropriate for use of the Pearson product-moment correlation coefficient are fully met.⁵³

3.6 | The relationship between cell size and enzyme activity signature at different stages of oocyte development

Plots of cell volume against GAPDH and MDH1 $^{cell}v_0$ for stage II, IV, and VI oocytes of animal 1 are shown

in Figure 6. As for animal 3 (Figure 3D), the whole-cell activity signature of GAPDH and MDH1 did not co-vary with cell size at stage VI of oogenesis (Figure 6, bottom row). Cell volume and $^{cell}v_0$ were also poorly correlated at stage II (Figure 6, top row). At stage IV, however, there was a very robust linear correlation between cell volume and the $^{cell}v_0$ of both GAPDH and MDH1 (Figure 6, middle row). To summarize, cell volume and $^{cell}v_0$ were poorly correlated at stage II, highly correlated at stage IV, and poorly correlated at stage VI. Therefore, in addition to programmed reduction of cell-to-cell heterogeneity of GAPDH and MDH1 $^{cell}v_0$ (Figure 4B), oogenesis may be characterized by a transient increase (at stage IV) of coupling between cell size control and the operation of

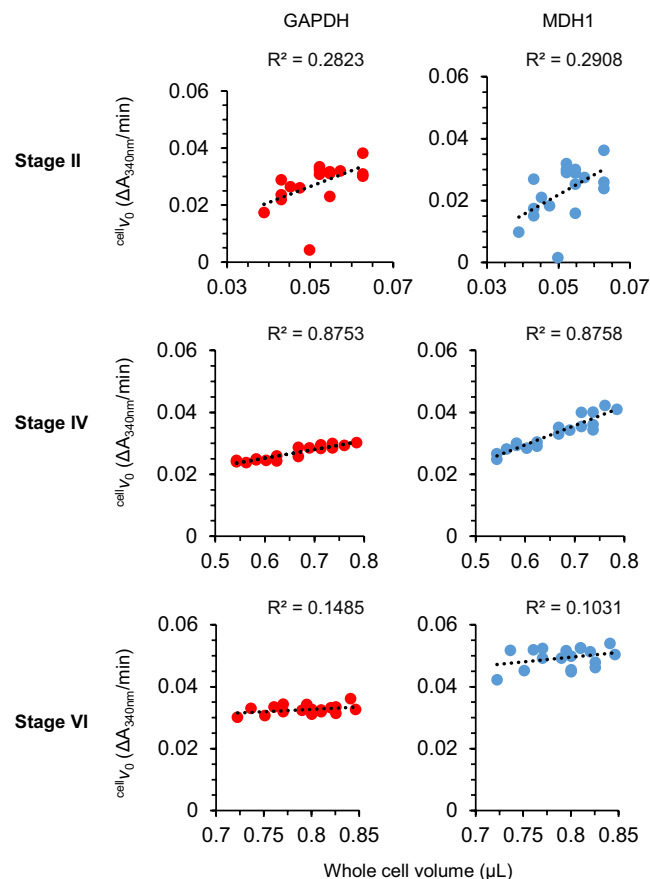


FIGURE 6 Relationship of cell volume to GAPDH and MDH1 $^{cell}v_0$ for oocytes at three stages of development. The data for GAPDH (red) and MDH1 (blue) are shown in the left and right panels, respectively. When considered as a temporal series, the data are consistent with developmental regulation of the strength of the relationship between cell volume and $^{cell}v_0$. The pattern is similar for GAPDH and MDH1: a robust increase of correlation strength from stage II to stage IV, followed by a stronger decline from stage IV to VI (compare top, middle, and bottom plots for each enzyme). Equations for the lines of best fit are presented in Table S2D. Note that the R^2 values shown here for stage VI oocytes of animal 1 approach those determined for stage VI oocytes of animal 3 (Figure 3D).

a module of metabolism that depends on GAPDH and MDH1 activity.

3.7 | Comparison of estimates of $^{cell}K_m$ and $^{cell}V_{max}$ between single oocytes

$^{cell}v_0$ is a signature of the kinetic behavior of the whole population of an enzyme in a cell. It can be used to gain insight into heterogeneity of the metabolic state of cells (Figures 1-6). Theoretically, profiling of Michaelis-Menten parameters such as K_m and V_{max} might also report on metabolic state variability (even if the existence of multiple enzyme isotypes in a cell precludes rigorous

analysis of catalytic mechanisms). To explore this possibility, Michaelis-Menten plots of substrate titrations into homogenates were used to obtain estimates of $^{cell}K_m$ and $^{cell}V_{max}$ for MDH1 in two stage VI cells (cells 8 and 16 of animal 2; $^{cell}v_0$ data in Figure 2). As exemplified by the data for cell 8, OAA titration into whole-cell homogenate yields a robust set of progress curves (Figure 7A). The values of $^{cell}K_m$ and $^{cell}V_{max}$ obtained from these curves differ between the oocytes by 3.12-fold and 2.63-fold, respectively (Figure 7B). Therefore, the usefulness of kinetic analysis for exploring cell-to-cell variability of metabolic state extends beyond assessment of initial rate.

4 | DISCUSSION

The key finding of this study is that whole-cell biochemical profiling of two metabolic enzymes can reveal physiological variation of enzyme activity state between individual cells of the same type. This variation is manifest in isolated oocytes as variation of GAPDH $^{cell}v_0$ between cells and variation of MDH1 $^{cell}v_0$ between cells. The activity signatures of GAPDH and MDH1 do not vary independently. Rather, they are positively correlated in three types of oocyte (at stages II, IV, and VI of development). It follows that the same regulatory system programs the $^{cell}v_0$ of GAPDH and MDH1.

The observed variability of enzyme activity signature between isolated oocytes of the same type is consistent with two working models of causation. One is that single-cell variability of $^{cell}v_0$ is observed in isolated oocytes because this variability is a feature of normal oogenesis (that is, isolated oocytes preserve normal *in vivo* variability of enzyme programming). In the second model, the variability is attributed to differences between cells in the penetrance of a response triggered by cell isolation and/or primary culture. This response modulates $^{cell}v_0$ and varies in strength between oocytes of the same type.

In terms of mechanism, both models of the cause of co-regulation of GAPDH and MDH1 activity can be extended to incorporate the concept of single-cell regulation by niche or microenvironment. The precedent here is that differences of *in vivo* niche can contribute to differences of metabolic programming between normal somatic cells of the same type and between cancer cells in a solid tumor.⁵⁴⁻⁵⁶ Variability of niche between oocytes is plausible considering the architecture of the oocyte follicle. Each follicle contains one oocyte and associated connective tissue elements, follicle cells, blood vessels, and nerves that are not directly shared with any other oocyte.^{9,11,57} Variability of any one of these features between oocyte follicles could underlie single-cell variability of regulatory

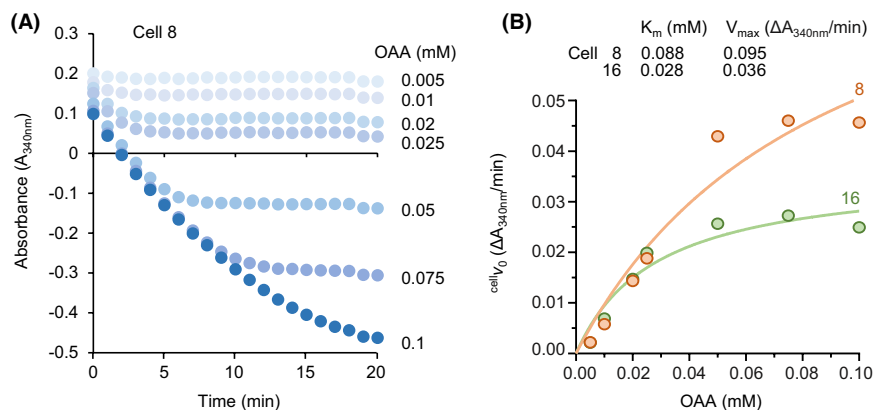


FIGURE 7 Profiling of MDH1 $^{cell}K_m$ and $^{cell}V_{max}$ from titrations of OAA into homogenates of two stage VI oocytes. (A) Representative set of progress curves at increasing concentrations of OAA (cell 8). The expected dependence of NADH consumption on OAA concentration is readily apparent. (B) Michaelis-Menten plot of data from OAA titration curves for the same amount of homogenate of cells 8 and 16. K_m and V_{max} were estimated using nonlinear regression for data fitting.

mechanisms that influence the activity signatures of oocyte GAPDH and MDH1.

The way that niche is expected to template oocyte to oocyte variability of GAPDH and MDH1 activity signatures differs between the model invoking $^{cell}v_0$ heterogeneity as hallmark of normal oogenesis (the developmental model) and the model in which $^{cell}v_0$ variability reflects variability of the response to isolation/primary culture (the stress model). Under the developmental model, matching of each oocyte to its in vivo niche partly involves metabolic adaptation by co-regulation of GAPDH and MDH1 v_0 . Under the stress model, matching of each oocyte to its niche shapes the wiring of cell defense systems that have GAPDH and MDH1 as their targets. Cell-to-cell variability of this wiring could account for the generation of variability of GAPDH and MDH1 $^{cell}v_0$ upon oocyte isolation. In addition, the higher correlation of GAPDH and MDH1 activity signatures in stage II compared to stage VI oocytes could reflect niche maturation during oogenesis. The latter process (as described for mammalian oocytes⁵⁸) would reduce niche variability and promote a metabolic state that does not demand tight coupling between GAPDH and MDH1 activity signatures, or does not effectively prime cell stress pathways that impinge on GAPDH and MDH1.

Many physiological inputs could contribute to the programming of GAPDH and MDH1 $^{cell}v_0$. The following speculations highlight one possibility. As noted in the introduction, enzyme oxidation state at redox-sensitive cysteines tunes the activity of both GAPDH and MDH1.^{21,29} Therefore, in addition to modulation of abundance (Figure 3B, C), control of enzyme oxidation state is a plausible mechanism for setting the strength of covariation of $^{cell}v_0$. Metabolic activity in the cell is linked to control of protein oxidation state in many ways. One is exposure to redox reactive chemical species (RRS). The intensity of

this exposure depends on the steady state level of RRS in the cell, which in turn depends on how they originate how and how they are removed. Cell-to-cell variability of niche could influence these processes in a way that affects covariation of GAPDH and MDH1 activity. Protein oxidation state is also controlled by systems that remove oxidative post-translational modifications. Cell-to-cell variability of niche could influence the function of proteins in these redox eraser systems. A difference between GAPDH and MDH1 in how strongly their activity is affected by oxidation could account for the weakness of the correlation of $^{cell}v_0$ for GAPDH and MDH1 compared to their correlation of abundance.

The physiological significance of coordinate regulation of GAPDH and MDH1 activity in oocytes has not been determined, but clear possibilities are suggested by what is known about metabolic programming in other cells. For example, in an osteosarcoma cell line the activity of MDH1 as a component of the malate aspartate shuttle partly depends on NADH produced by GAPDH. This dependency intensifies under conditions of mitochondrial dysfunction, as does the interaction of GAPDH and MDH1 measured by co-immunoprecipitation and co-localization assays.³² Coordinated fluctuation of GAPDH and MDH1 activity may function in this context to integrate the programming of cytosolic and mitochondrial metabolism.

In the present study, activity profiling of just two enzymes in whole-cell lysates has revealed a previously unknown axis of variability between oocytes of the same type. This success encourages further use of multienzyme activity profiling to characterize cell-to-cell variability of metabolic phenotypes. Work using the oocyte system could be extended to address two general questions. 1. Can it be informative to know the activity signatures of more than two enzymes? The answer to this question

could be obtained by studying isocitrate dehydrogenase I and the pentose phosphate pathway enzymes glucose 6-phosphate dehydrogenase and phosphogluconate dehydrogenase (respectively, IDH1, G6PD, and PGD; in pilot studies, all exhibited robust activity in ensemble homogenates of stage V/VI oocytes). 2. Can understanding of cell-to-cell variability of enzyme activity signatures be refined by separately characterizing the nuclear and cytoplasmic pools of enzymes? This question will be straightforward to answer because GAPDH, MDH1, IDH1, G6PD, and PGD are abundant in the oocyte nucleus^{17,18} and in our hands exhibit high activity in homogenates of oil-isolated whole nucleus and whole cytoplasm. A possibility we have not addressed is whether the cells of a type exist in a continuum of states defined by the activity profile of an enzyme, as opposed to a set of distinct sub-states with sub-groups of cells clustering around different averages of enzyme activity (e.g., high- and low-activity subpopulations of stage VI oocytes). In future work, profiling of larger numbers of cells could expose such discontinuous distributions.

What has already been discovered using the oocyte system encourages our expectation that multi-enzyme activity signature profiling will also advance understanding of developmental processes in mammals. Such a research program could reasonably build on recent advances in ultrahigh throughput methods for directed evolution of enzymes. These advances include assay of enzyme activity in lysates of single *E. coli* cells using a chemical sensor of NADH and the use of a fluorescent protein-based sensor of the NAD⁺:NADH ratio to detect enzyme activity in reaction droplets.^{59,60}

AUTHOR CONTRIBUTIONS

MCS. developed the initial concept and design of this research program, and performed the animal work, cell isolation, and analysis of proteomics data. GSG. contributed to hypothesis development and planning of experimental approaches, and refined and performed the enzyme assays and calculated estimates of kinetic parameters. Both authors were involved in interpreting the data and drafting and revising the manuscript.

ACKNOWLEDGMENTS

The authors thank Chelsea Gates for technical assistance and Helen Tang for technical advice and discussions about the data. Analytical services were provided by Dr. Jack Moore at the Alberta Proteomics and Mass Spectrometry Facility, Faculty of Medicine and Dentistry, University of Alberta. We thank Dr. Richard Fahlman for expert advice regarding the LC-MS analysis, and Dr. Paul LaPointe for plate reader access. This research was supported by a Project Grant to MCS from the Canadian Institutes of Health Research (FRN 148760). GSG was supported in

part by an Undergraduate Student Research Award from the Natural Sciences and Engineering Research Council of Canada.

CONFLICT OF INTEREST

The authors declare no conflicts of interest.

DATA AVAILABILITY STATEMENT

The data that support the findings of this study are available in supplementary material of this article.

ORCID

Michael C. Schultz  <https://orcid.org/0000-0002-2721-387X>

REFERENCES

1. Wagner A, Regev A, Yosef N. Revealing the vectors of cellular identity with single-cell genomics. *Nat Biotechnol.* 2016;34(11):1145-1160.
2. Gerbin KA, Grancharova T, Donovan-Maiye RM, et al. Cell states beyond transcriptomics: integrating structural organization and gene expression in hiPSC-derived cardiomyocytes. *Cell Syst.* 2021;12(6):670-687.
3. Rautenstrauch P, Vlot AHC, Saran S, Ohler U. Intricacies of single-cell multi-omics data integration. *Trends Genet.* 2022;38(2):128-139.
4. Trefts E, Gannon M, Wasserman DH. The liver. *Curr Biol.* 2017;27(21):R1147-R1151.
5. Artyomov MN, Van den Bossche J. Immunometabolism in the single-cell era. *Cell Metab.* 2020;32(5):710-725.
6. Hrovatin K, Fischer DS, Theis FJ. Toward modeling metabolic state from single-cell transcriptomics. *Mol Metab.* 2022;57:101396.
7. Kovarik ML, Allbritton NL. Measuring enzyme activity in single cells. *Trends Biotechnol.* 2011;29(5):222-230.
8. Wudl L, Paigen K. Enzyme measurements on single cells. *Science.* 1974;184(4140):992-994.
9. Rasar MA, Hammes SR. The physiology of the *Xenopus laevis* ovary. *Methods Mol Biol.* 2006;322:17-30.
10. Ferrell JE Jr. *Xenopus* oocyte maturation: new lessons from a good egg. *Bioessays.* 1999;21(10):833-842.
11. Dumont JN. Oogenesis in *Xenopus laevis* (Daudin). I. Stages of oocyte development in laboratory maintained animals. *J Morphol.* 1972;136(2):153-179.
12. Dworkin MB, Dworkin-Rastl E. Metabolic regulation during early frog development: glycogenic flux in *Xenopus* oocytes, eggs, and embryos. *Dev Biol.* 1989;132(2):512-523.
13. Sadler SE, Maller JL. The development of competence for meiotic maturation during oogenesis in *Xenopus laevis*. *Dev Biol.* 1983;98(1):165-172.
14. Jessup C, Ozon R. How does *Xenopus* oocyte acquire its competence to undergo meiotic maturation? *Biol Cell.* 2004;96(3):187-192.
15. White MR, Garcin ED. D-Glyceraldehyde-3-phosphate dehydrogenase structure and function. *Subcell Biochem.* 2017;83:413-453.
16. Borst P. The malate-aspartate shuttle (Borst cycle): how it started and developed into a major metabolic pathway. *IUBMB Life.* 2020;72(11):2241-2259.

17. Kırılı K, Karaca S, Dehne HJ, et al. A deep proteomics perspective on CRM1-mediated nuclear export and nucleocytoplasmic partitioning. *Elife*. 2015;4:e11466.
18. Wühr M, Güttler T, Peshkin L, et al. The nuclear proteome of a vertebrate. *Curr Biol*. 2015;25(20):2663-2671.
19. Kim EY, Kim WK, Kang HJ, et al. Acetylation of malate dehydrogenase 1 promotes adipogenic differentiation via activating its enzymatic activity. *J Lipid Res*. 2012;53(9):1864-1876.
20. Wang YP, Zhou W, Wang J, et al. Arginine methylation of MDH1 by CARM1 inhibits glutamine metabolism and suppresses pancreatic cancer. *Mol Cell*. 2016;64(4):673-687.
21. Guo X, Park JE, Gallart-Palau X, Sze SK. Oxidative damage to the TCA cycle enzyme MDH1 dysregulates bioenergetic enzymatic activity in the aged murine brain. *J Proteome Res*. 2020;19(4):1706-1717.
22. Singh P, Salih M, Leddy JJ, Tuana BS. The muscle-specific calmodulin-dependent protein kinase assembles with the glycolytic enzyme complex at the sarcoplasmic reticulum and modulates the activity of glyceraldehyde-3-phosphate dehydrogenase in a Ca²⁺/calmodulin-dependent manner. *J Biol Chem*. 2004;279(34):35176-35182.
23. Ang J, Gibson B, Snider J, Jenkins CM, Han X, Gross RW. Submicromolar concentrations of palmitoyl-CoA specifically thioesterify cysteine 244 in glyceraldehyde-3-phosphate dehydrogenase inhibiting enzyme activity: a novel mechanism potentially underlying fatty acid induced insulin resistance. *Biochemistry*. 2005;44(35):11903-11912.
24. Bond ST, Howlett KF, Kowalski GM, et al. Lysine post-translational modification of glyceraldehyde-3-phosphate dehydrogenase regulates hepatic and systemic metabolism. *FASEB J*. 2017;31(6):2592-2602.
25. Kulkarni RA, Worth AJ, Zengeya TT, et al. Discovering targets of non-enzymatic acylation by thioester reactivity profiling. *Cell Chem Biol*. 2017;24(2):231-242.
26. Kornberg MD, Bhargava P, Kim PM, et al. Dimethyl fumarate targets GAPDH and aerobic glycolysis to modulate immunity. *Science*. 2018;360(6387):449-453.
27. Zhong XY, Yuan XM, Xu YY, et al. CARM1 Methylates GAPDH to regulate glucose metabolism and is suppressed in liver cancer. *Cell Rep*. 2018;24(12):3207-3223.
28. Galván-Peña S, Carroll RG, Newman C, et al. Malonylation of GAPDH is an inflammatory signal in macrophages. *Nat Commun*. 2019;10(1):338.
29. Tossounian MA, Zhang B, Gout I. The writers, readers, and erasers in redox regulation of GAPDH. *Antioxidants (Basel)*. 2020;9(12):1288.
30. Martens GA, Jiang L, Verhaeghen K, et al. Protein markers for insulin-producing beta cells with higher glucose sensitivity. *PLoS One*. 2010;5(12):e14214.
31. Hanse EA, Ruan C, Kachman M, Wang D, Lowman XH, Kelekar A. Cytosolic malate dehydrogenase activity helps support glycolysis in actively proliferating cells and cancer. *Oncogene*. 2017;36(27):3915-3924.
32. Gaude E, Schmidt C, Gammage PA, et al. NADH shuttling couples cytosolic reductive carboxylation of glutamine with glycolysis in cells with mitochondrial dysfunction. *Mol Cell*. 2018;69(4):581-593.e7.
33. Montllor-Albalade C, Kim H, Thompson AE, Jonke AP, Torres MP, Reddi AR. Sod1 integrates oxygen availability to redox regulate NADPH production and the thiol redoxome. *Proc Natl Acad Sci U S A*. 2022;119(1):e2023328119.
34. Uhlén M, Fagerberg L, Hallström BM, et al. Proteomics. Tissue-based map of the human proteome. *Science*. 2015;347(6220):1260419.
35. Crane RF, Ruderman JV. Using *Xenopus* oocyte extracts to study signal transduction. *Methods Mol Biol*. 2006;322:435-443.
36. Liu XS, Liu XJ. Oocyte isolation and enucleation. *Methods Mol Biol*. 2006;322:31-41.
37. Gall JG, Murphy C, Callan HG, Wu ZA. Lampbrush chromosomes. *Methods Cell Biol*. 1991;36:149-166.
38. Velick SF. Glyceraldehyde-3-phosphate dehydrogenase from muscle. *Methods Enzymol*. 1955;1:401-406.
39. Kemmer G, Keller S. Nonlinear least-squares data fitting in excel spreadsheets. *Nat Protoc*. 2010;5(2):267-281.
40. Mounaji K, Vlasi M, Errais NE, Wegnez M, Serrano A, Soukri A. In vitro effect of metal ions on the activity of two amphibian glyceraldehyde-3-phosphate dehydrogenases: potential metal binding sites. *Comp Biochem Physiol B Biochem Mol Biol*. 2003;135(2):241-254.
41. Paine PL, Johnson ME, Lau YT, Tluczek LJ, Miller DS. The oocyte nucleus isolated in oil retains in vivo structure and functions. *Biotechniques*. 1992;13(2):238-246.
42. Han ZZ, Schultz MC. The protein interactome of a nanoparticle population in whole cytoplasm under near-native conditions: a pilot study. *Particle & Particle Systems Characterization*. 2022;39(4):2100283.
43. Board M, Humm S, Newsholme EA. Maximum activities of key enzymes of glycolysis, glutaminolysis, pentose phosphate pathway and tricarboxylic acid cycle in normal, neoplastic and suppressed cells. *Biochem J*. 1990;265(2):503-509.
44. Ferrell JE Jr, Machleder EM. The biochemical basis of an all-or-none cell fate switch in *Xenopus* oocytes. *Science*. 1998;280(5365):895-898.
45. Baltus E, Hanocq-Quertier J, Brachet J. Isolation of deoxyribonucleic acid from the yolk platelets of *Xenopus laevis* oocyte. *Proc Natl Acad Sci U S A*. 1968;61(2):469-476.
46. Gurdon JB, Wickens MP. The use of *Xenopus* oocytes for the expression of cloned genes. *Methods Enzymol*. 1983;101:370-386.
47. Tokmakov AA, Hashimoto T, Hasegawa Y, Iguchi S, Iwasaki T, Fukami Y. Monitoring gene expression in a single *Xenopus* oocyte using multiple cytoplasmic collections and quantitative RT-PCR. *FEBS J*. 2014;281(1):104-114.
48. Richard A, Boullu L, Herbach U, et al. Single-cell-based analysis highlights a surge in cell-to-cell molecular variability preceding irreversible commitment in a differentiation process. *PLoS Biol*. 2016;14(12):e1002585.
49. Mojtahedi M, Skupin A, Zhou J, et al. Cell fate decision as high-dimensional critical state transition. *PLoS Biol*. 2016;14(12):e2000640.
50. Semrau S, Goldmann JE, Soumillon M, Mikkelsen TS, Jaenisch R, van Oudenaarden A. Dynamics of lineage commitment revealed by single-cell transcriptomics of differentiating embryonic stem cells. *Nat Commun*. 2017;8(1):1096.
51. Stumpf PS, Smith RCG, Lenz M, et al. Stem cell differentiation as a non-Markov stochastic process. *Cell Syst*. 2017;5(3):268-282.e7.
52. Ando T, Kato R, Honda H. Identification of an early cell fate regulator by detecting dynamics in transcriptional heterogeneity

- and co-regulation during astrocyte differentiation. *NPJ Syst Biol Appl.* 2019;5:18.
53. Goodwin LD, Leech NL. Understanding correlation: factors that affect the size of r. *J Exp Edu.* 2006;74(3):249-266.
 54. Zheng L, Kelly CJ, Colgan SP. Physiologic hypoxia and oxygen homeostasis in the healthy intestine. A review in the theme: cellular responses to hypoxia. *Am J Physiol Cell Physiol.* 2015;309(6):C350-C360.
 55. Kietzmann T. Metabolic zonation of the liver: the oxygen gradient revisited. *Redox Biol.* 2017;11:622-630.
 56. Pavlova NN, Zhu J, Thompson CB. The hallmarks of cancer metabolism: still emerging. *Cell Metab.* 2022;34(3):355-377.
 57. Lametschwandtner A, Minnich B. Microvascular anatomy of ovary and oviduct in the adult African clawed toad (*Xenopus laevis* DAUDIN, 1802)-histomorphology and scanning electron microscopy of vascular corrosion casts. *Anat Histol Embryol.* 2020;49(6):742-748.
 58. Yang L, Ng HH. The making of an ovarian niche. *Science.* 2021;373(6552):282-283.
 59. Gielen F, Hours R, Emond S, Fischlechner M, Schell U, Hollfelder F. Ultrahigh-throughput-directed enzyme evolution by absorbance-activated droplet sorting (AADS). *Proc Natl Acad Sci USA.* 2016;113(47):E7383-E7389.
 60. Lindenburg L, Hollfelder F. "NAD-display": ultrahigh-throughput in vitro screening of NAD(H) dehydrogenases using bead display and flow cytometry. *Angew Chem Int ed Engl.* 2021;60(16):9015-9021.

SUPPORTING INFORMATION

Additional supporting information can be found online in the Supporting Information section at the end of this article.

How to cite this article: Gill GS, Schultz MC. Multienzyme activity profiling for evaluation of cell-to-cell variability of metabolic state. *FASEB BioAdvances.* 2022;4:709-723. doi: [10.1096/fba.2022-00073](https://doi.org/10.1096/fba.2022-00073)